Journal of Marine Research, 51, 819–842, 1993

Phytoplankton bloom and the vertical thermal structure of the upper ocean

by Malgorzata Stramska[1] and Tommy D. Dickey[1]

ABSTRACT

Local heating rate within the oceanic mixed layer (ML) depends not only on the amount of solar radiation incident on the sea surface, but also on the vertical distribution of the irradiance in the water column. We have evaluated the effect of a phytoplankton bloom on mixed layer depth and temperature at a high latitude site near Iceland. The level 2½ version of the Mellor-Yamada (1982) turbulence scheme has been modified to include the vertical distribution of irradiance. This has allowed the investigation of the ML temperature and stability structure resulting from both physical and biological effects. An important part of the model is the parameterization of pigment-dependence which affects the spectral attenuation coefficient for downwelling irradiance as proposed by Morel (1988). Concurrent, high temporal resolution time series of physical and bio-optical data were used for the model. These data were acquired using a mooring deployed during the spring of 1989. We have estimated that the increase of phytoplankton abundance induced an increase of the sea surface temperature by about 0.2°C at the mooring site. This led to stronger near-surface thermal stratification and shallower mixed layers. The dependence of the upper layer thermal structure on biology is more important when vertical mixing is weaker and when phytoplankton concentrations are higher.

1. Introduction

It has long been suggested that the annual cycle of phytoplankton populations is driven by the seasonal periodicity of physical conditions in the ocean. According to classical models (e.g., Gran and Braarud, 1935; Sverdrup, 1953), the spring bloom is initiated by the sudden shoaling of the mixed layer. It is argued that phytoplankton cells are essentially trapped in the mixed layer, exposed to higher average light intensity, and respond with increasing growth rates. Thus, the important physical factors governing the bloom development are intensity of the solar radiation penetrating the water column and the mixed layer dynamics. Intensive mixing can reduce phytoplankton growth by increasing the depth of the mixed layer, which in turn causes light limitation.

1. Ocean Physics Group, Department of Geological Sciences, University of Southern California, Los Angeles, California, 90089-0740, U.S.A.

On the other hand, it is possible that biological processes can affect the thermal structure and the dynamics of the upper ocean. Local heating rate depends not only on the amount of the solar radiation incident on the sea surface, but also on the vertical distribution of irradiance in the water column. Since pigmented phytoplankton cells are major absorbers and scatterers of light in the open ocean (e.g., Jerlov, 1976), they regulate the penetration of the radiant energy in the water. Nonuniformities in the vertical chlorophyll distribution may lead to nonuniformities in the light absorption and local heating (Lewis *et al.,* 1983).

Absorption of light in oceanic water is wavelength dependent and varies in time and space due to the variability of the pigment concentration (e.g., Baker and Smith, 1982; Kirk, 1983; Morel, 1988; Sathyendranath and Platt, 1988). Nonetheless, models of the upper ocean dynamics have often employed simple irradiance penetration schemes using exponential vertical distributions of the downward irradiance or have assumed heat flux solely as a surface input. Different penetrative irradiance parameterizations have been shown to affect the predicted thermal structure of the upper ocean (Dickey and Simpson, 1983; Simpson and Dickey, 1981a, b; Woods and Barkmann, 1986). Numerical models suggest that studies of the mixed layer should include the parametrization of light absorption accounting for the variability of the pigment concentration (e.g., Zaneveld *et al.,* 1981; Lewis *et al.,* 1983, 1990; Simonot *et al.,* 1988; Sathyendranath *et al.,* 1991). In addition, experimental data indicate that biomass can influence the thermal structure and mixing depth in lakes (Mazumder *et al.,* 1990).

A one-dimensional model coupling dynamical-biooptical components is utilized for the present study. In this model, the propagation of the radiant energy is a function of wavelength and phytoplankton concentration as proposed by Morel (1988). The optical model is incorporated in the level 2½ version of the Mellor and Yamada turbulent closure scheme (e.g., Mellor and Yamada, 1982). The model is ideal for the investigation of the temporal variability of the vertical temperature and stability structure of the mixed layer resulting from both physical and biological effects. The purpose here is to examine the physical/biological feedbacks during the development of the seasonal thermocline and the spring phytoplankton bloom. The subject of this paper is closely related to the understanding of the initiation of the springtime phytoplankton bloom, because even small changes in the water stability may be important for the timing and magnitude of the bloom. The model uses high temporal resolution field data obtained during two months in the spring of 1989 at an open ocean site south of Iceland during the Marine Light in the Mixed Layer (MLML) experiment.

2. Field experiment

Time-series data were obtained with multi-variable moored systems (MVMS, Dickey *et al.,* 1991, 1993) and a surface meteorological system. The major strength of

this data set is that it provides concurrent measurements of physical and bio-optical parameters, thus facilitating the study of interactions between biological and physical processes in the open ocean.

The measurements were carried out from April 13 through June 12, 1989 (Julian days 103–163), in the North Atlantic (59° 29′ N, 20° 50′ W), as a part of the Marine Light in the Mixed Layer (MLML) program. The details of the methodologies are given elsewhere (Dickey *et al.,* 1991, 1993; Marra *et al.,* 1992), thus only a short description relevant to our study is presented here. The sensor suite for the MVMS included: a vector measuring current meter (VMCM, Weller and Davis, 1980), a thermistor for water temperature measurements, a PAR sensor with a spherical collector for measuring scalar irradiance within the visible spectral range (Booth, 1976), a beam transmissometer (light wavelength of 660 nm, Bartz *et al.,* 1978), an *in situ* stimulated fluorescence sensor (blue excitation filter and red emission filter, Bartz *et al.,* 1988), and a pulsed electrode dissolved oxygen sensor (Langdon, 1984). The MVMS systems sampled at nominal fixed depths of 10, 30, 50, 90, 110, 150 and 250 m. Deeper water temperatures were measured at 200, 350, 400, 450, 500, 550, 650, 700, and 750 m using thermistors. In addition, meteorological measurements included: wind speed and direction, barometric pressure, air and sea surface temperatures, and incident solar radiation (250–2500 nm). The basic sampling rate for the MVMS systems was either 1 min (at 10, 50, 90, 150 m) or 7.5 min (at 30, 110, 250 m). The meteorological data and the deep water temperatures were acquired at 7.5 min intervals. The data set was processed to produce 15 min averaged time series which were used for this study. Since the surface water temperature sensor failed after a few weeks of the experiment, we have used the temperature from 10 m depth to calculate heat fluxes.

3. Model formulation

The level 2½ version of the Mellor-Yamada model was employed (Mellor and Yamada, 1974, 1982; Mellor and Durbin, 1975; Blumberg and Mellor, 1983). This model belongs to the class of differential models, opposed to bulk integrated models, and enables computation of vertical profiles of turbulent variables. Thus, the time dependent vertical distribution of the solar radiation could be incorporated into the model. It is also important that this model has a realistic, stability dependent eddy diffusivity parametrization, allowing interaction between heating and turbulence structure. Only basic features of the Mellor-Yamada model are summarized here as details may be found in papers cited above.

The model is based on the solution of mean thermodynamic and momentum equations as well as turbulence equations, with assumptions for closing the system of equations. For a horizontally homogeneous ocean with no average vertical water

movement, the equations of conservation of momentum and heat may be written as:

$$\begin{aligned}
\frac{\partial U}{\partial t} - f(V - V_g) &= \frac{\partial}{\partial z}\left[(K_M + \nu_M)\frac{\partial U}{\partial z}\right] \\
\frac{\partial V}{\partial t} + f(U - U_g) &= \frac{\partial}{\partial z}\left[(K_M + \nu_M)\frac{\partial V}{\partial z}\right] \\
\frac{\partial T}{\partial t} &= \frac{\partial}{\partial z}\left[(K_H + \nu_H)\frac{\partial T}{\partial z}\right] + \frac{1}{\rho_0 c_p}\frac{\partial E_d}{\partial z}
\end{aligned} \tag{1}$$

where t is time, z the vertical coordinate, U and V the mean horizontal velocity components, T the temperature, E_d the downwelling irradiance, f the Coriolis parameter, K_M and K_H the eddy coefficients for vertical turbulent diffusion, ν_M and ν_H the coefficients for ambient viscosity and diffusion, ρ_o the mean water density, and c_p the specific heat of water. For simplicity, the geostrophic current components U_g and V_g are taken to be zero. The equation set (1) is closed using the following formulas for eddy coefficients:

$$\begin{aligned}
K_M &= l\, q\, S_M \\
K_H &= l\, q\, S_H
\end{aligned} \tag{2}$$

where l is the turbulent length scale, $q^2/2$ is the turbulent kinetic energy (*TKE*), and S_M and S_H are the stability functions dependent on the local Richardson number (*Ri*). The Richardson number, defined as the ratio of negative turbulent buoyancy production to the shear production may be expressed as:

$$Ri = \frac{K_H \frac{g}{\rho}\frac{\partial \rho}{\partial z}}{K_M\left[\left(\frac{\partial U}{\partial z}\right)^2 + \left(\frac{\partial V}{\partial z}\right)^2\right]} \tag{2}$$

where g is the acceleration due to gravity.

The *TKE* is determined from the equation:

$$\frac{\partial (q^2/2)}{\partial t} = \frac{\partial}{\partial z}\left[\left(K_q \frac{\partial (q^2/2)}{\partial z}\right)\right] + K_M\left[\left(\frac{\partial U}{\partial z}\right)^2 + \left(\frac{\partial V}{\partial z}\right)^2\right] + K_H \frac{g}{\rho}\frac{\partial \rho}{\partial z} - q^3/cl \tag{3}$$

where K_q the coefficient for the vertical diffusion of *TKE* is taken proportional to K_M. The constant c scales with the dissipation length scale. To determine the distribution of water density ρ, the equation of state is used with the assumption that the contributions of salinity changes to water density variability are negligible. Both historical data from the region (Emery and Dewar, 1982) and our salinity measurements from the mooring (not shown here) justify this assumption. Note also that the equation of heat conservation differs from that used by Mellor and Yamada, because

the vertical gradient of downwelling irradiance E_d is included. We will describe this term in greater detail in a later paragraph.

Importantly, the results of our calculations are compared with actual ocean measurements on appropriate time scales. Boundary conditions are provided from our experimental data which contain a broad spectrum of variability. Wind stress was estimated as:

$$\tau = \rho_a c_D u \mathbf{u} \tag{4}$$

where $\mathbf{u}$ is the wind speed, ρ_a is the density of air and c_D is the drag coefficient calculated from a bulk aerodynamic formula (Large and Pond, 1982). The heat flux is the sum of the heat leaving directly from the water surface (loss), and the solar radiation absorbed in the water column (gain). The heat loss is the sum of the latent, sensible and longwave radiative heat fluxes. Surface heat fluxes are calculated using standard bulk formulas (Large and Pond, 1982; Geernaert, 1990), a net longwave radiation formula (Bunker, 1976; Fung *et al.,* 1984), and air-sea meteorological data from the MLML experiment. The humidity sensor failed; thus proxy air humidity data were utilized. These data were collected during the springtime period of 1989 at nearby Ocean Station Lima (57N, 20W).

An important feature of our model is the detailed parameterization of the solar irradiance which penetrates into the water column. It should be noted that parameterizations of radiant energy attenuation, which are commonly used in dynamical models, are based on optical measurements averaged vertically in space and in time and are characterized according to optical water type (Jerlov, 1976). They do not take into account specific temporary oceanic conditions, and typically do not compare favorably with observed vertical profiles of irradiance (e.g., Siegel and Dickey, 1987).

In our model, the vertical profiles of irradiance were calculated as follows. First, we obtained from the experiment time series of the incident solar radiation (250–2500 nm) just above the water surface. Using these data and the information on the average spectral composition of the solar irradiance (e.g., Bird *et al.,* 1983; Bird, 1984), we calculated the radiative energy in specified spectral bands. A bandwidth of 5 nm for the visible light and broader bandwidths outside that spectral region were used. The derived spectral distribution of surface irradiance, compares well with empirical results of other authors; that is, about 50% of the solar radiation is composed of visible light (Kishino *et al.,* 1986; Smith and Baker, 1986; Siegel and Dickey, 1987).

As a next step, we calculated vertical profiles of the spectral irradiance beneath the water surface assuming that about 94% of the radiative energy penetrates through the surface and that the transmittance is wavelength independent (Payne, 1972; Smith and Baker, 1986; Siegel and Dickey, 1987). We also assumed that there are two distinct ways of describing the fate of the solar radiative energy beneath the

water surface. First, the radiant energy outside the visible region is attenuated by water molecules only, and the effects of phytoplankton are negligible. The irradiance profiles in these spectral regions were calculated using the data compiled by Smith and Baker (1981), and Palmer and Williams (1974). According to these calculations, about half of the solar energy which transferred through water surface is absorbed in the top 1 m of the water column. The other half, the radiant energy from the visible spectral range, penetrates deeper into the water and its fate depends strongly on the phytoplankton abundance. The vertical profiles of irradiance in that spectral range were calculated following the model developed by Morel (1988). According to his model the vertical diffuse attenuation coefficient $K_d(\lambda)$ in units of m^{-1} is given by:

$$K_d(\lambda) = K_W(\lambda) + \kappa(\lambda)C^{\alpha(\lambda)} \tag{5}$$

where λ is the wavelength in vacuo, $K_W(\lambda)$ is the diffuse attenuation coefficient for pure seawater in m^{-1}, $\kappa(\lambda)$ and $\alpha(\lambda)$ are statistically derived empirical coefficients, and C is the chlorophyll concentration in mg m^{-3}. The vertical profiles of chlorophyll concentration were taken from the linear interpolation of our mooring fluorometric measurements, which were made at a number of fixed depths. Prior to performing these calculations, the fluorometric data were converted to chlorophyll concentrations using the calibration done in the laboratory before the deployment of the mooring (see Dickey *et al.,* 1993 and Marra *et al.,* 1992 for details). In order to remove the variability related to photoadaptive responses of phytoplankton (e.g., Stramska and Dickey, 1992), the data were filtered using a 24 hour moving average filter. Note also that in equation (1) we approximated the irradiance gradient in the water column as the gradient of downwelling irradiance E_d. The error in ignoring the upwelling irradiance (E_u) is relatively small since the ratio of E_u/E_d is typically on the order of 3%, and not greater than 10% (Kirk, 1983).

For the purpose of numerical calculations, Eqs. (1) were transformed into finite-difference equations using the implicit Crank-Nicholson scheme (Richtmyer and Morton, 1967). Since we were interested in the effects of irradiance attenuation on the structure of the mixed layer, the vertical grid spacing was optimized to give high vertical resolution near the water surface. The distance between computational grid points increased with depth according to a geometrical progression. The interval was 0.04 m at the surface and there were 301 levels down to a depth of 740 m. The time step was 15 minutes, the same as the interval between averaged experimental data.

4. Results

The details of the experimental results are reported in a separate paper (Dickey *et al.,* submitted). A brief summary of data relevant to the modeling study is given below. Figures 1 and 2 provide an overview of the meteorological and dynamical conditions at the mooring site. Throughout the experiment, the daily maximum

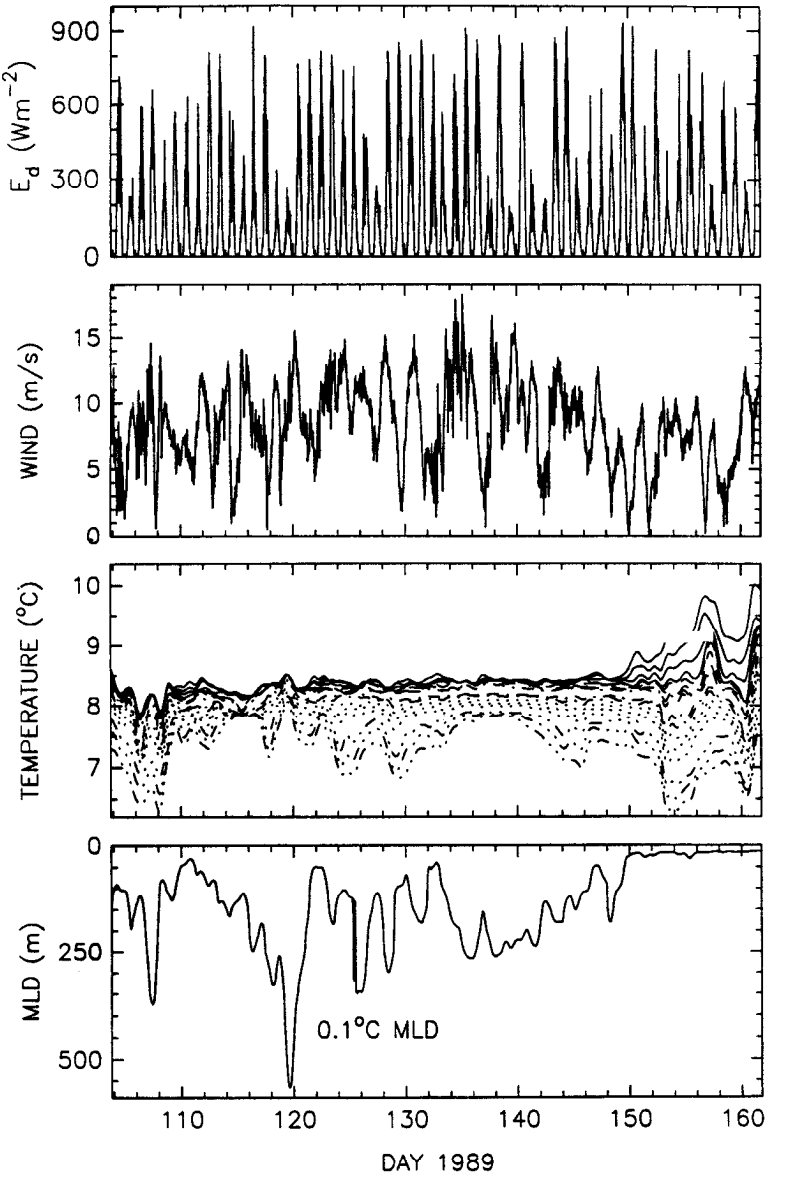

Figure 1. Time series of surface irradiance (E_d), wind speed, water temperature at 16 depths (10, 30, 50, 90, 110, 150, 200, 250, 350, 400, 450, 500, 550, 650, 700, and 750 m), and mixed layer depth (MLD). These data were collected during the MLML 1989 experiment and are 15-min averages.

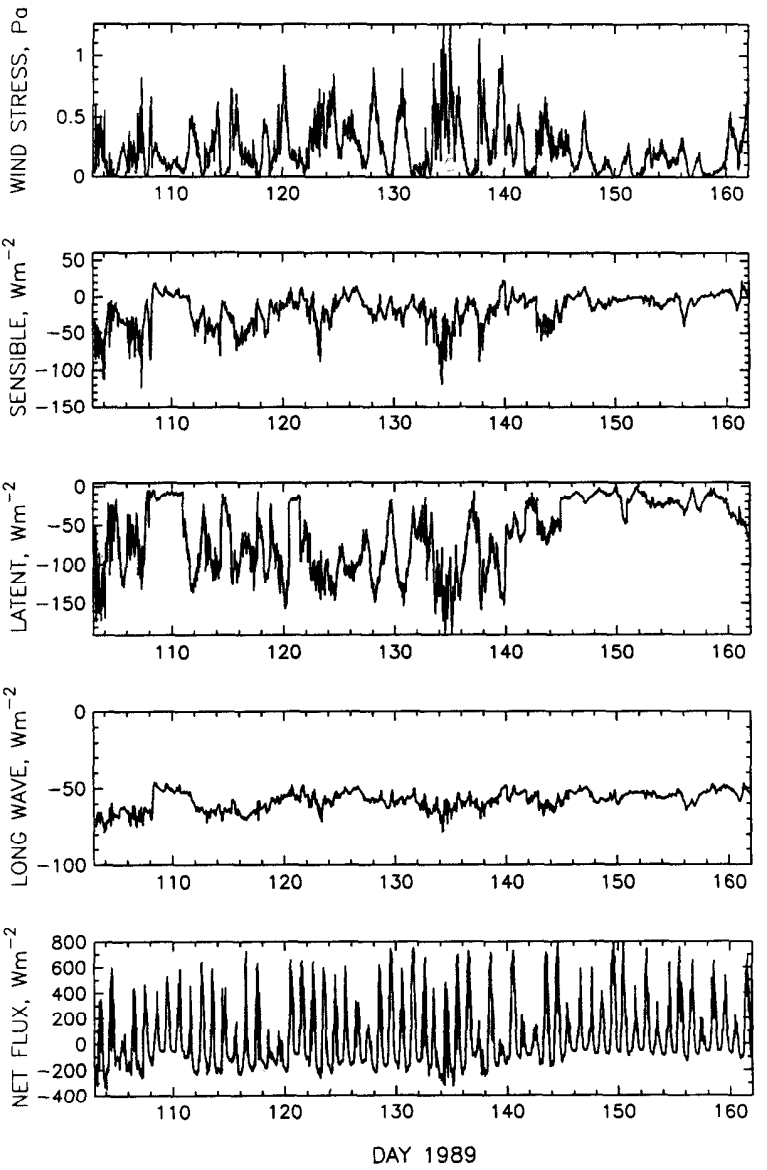

Figure 2. Time series of the wind stress, sensible heat flux, latent heat flux, net longwave heat flux, and surface net heat flux.

incoming solar radiation varied between 200 and 900 W m^{-2}, depending on cloudiness. Winds at times exceeded 15 m/sec. The mixed layer depth (MLD) is defined here as the depth at which the temperature change from the surface is 0.1°C. The estimates of the MLD may not be very exact, especially when the surface waters were

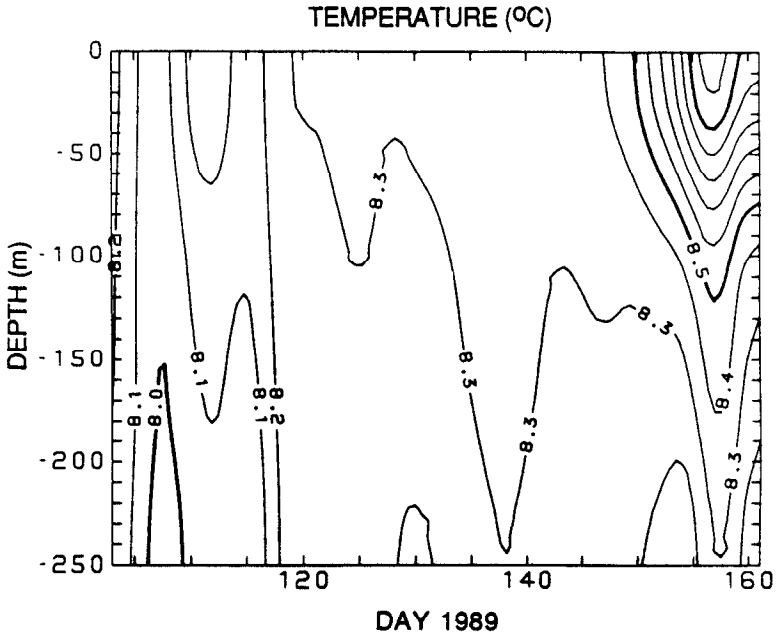

Figure 3. Depth versus time contours of measured water temperature.

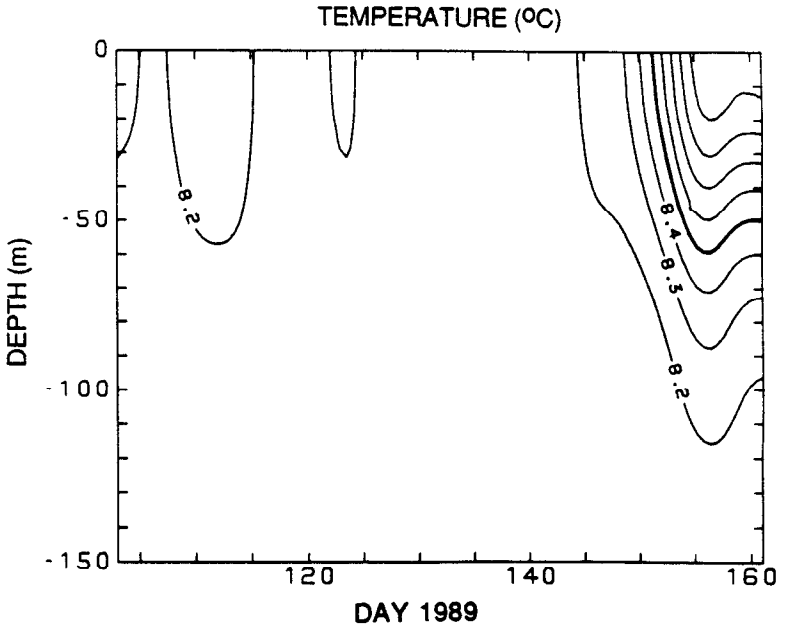

Figure 4. Water temperature contours after subtracting temperature variability at 150 m.

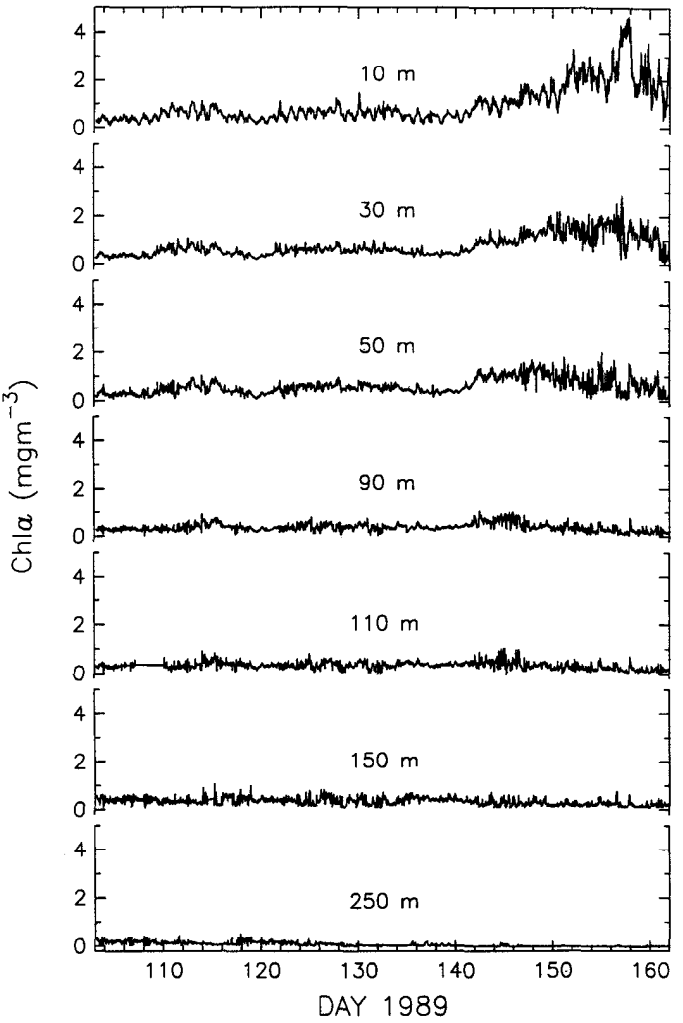

Figure 5. (a) Time series (b) contour plot of the fluorometrically determined concentration of chlorophyll a (mg m^{-3}).

warming, because of relatively wide spacing in standard mooring depths. Nevertheless, the plot of the MLD versus time shows that at the beginning of the experiment the temperature was nearly uniform down to about 100 m. During the course of the experiment, episodic events of shallowing and deepening of the mixed layer occurred. These events likely reflect a balance of heat gain and losses in the upper water as well as advection of warmer and cooler waters past the site. The seasonal temperature stratification became evident around day 145 and was coincident with some decrease of the wind speed (Fig. 1). Current speed varied between 0.2 and 0.9 m/sec during the course of the experiment (not shown).

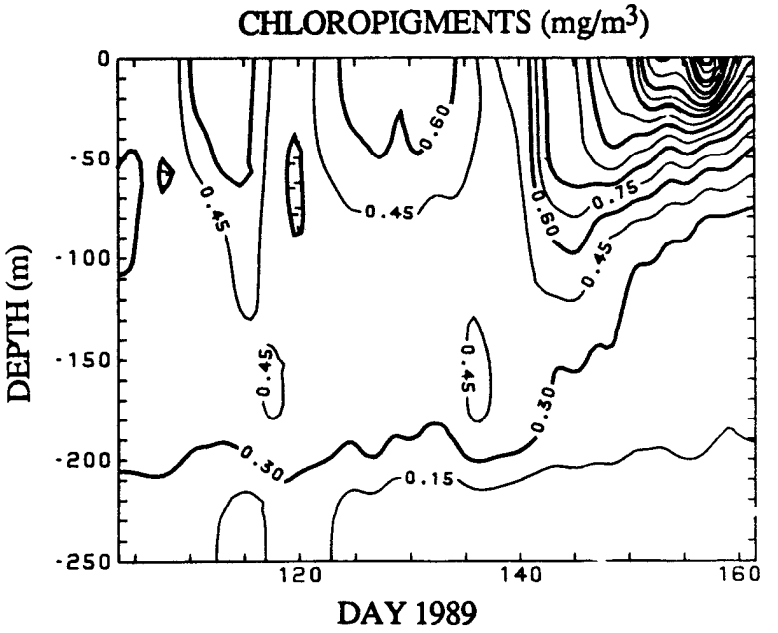

Figure 5. (Continued)

Wind stress and heat fluxes estimated for the MLML experiment are shown in Figure 2. The heat fluxes were estimated using bulk formulas and the uncertainty of the results may be as much as 20% (e.g., Bunker, 1976). In addition, some uncertainty was introduced by the fact that we did not have direct measurements of air humidity at the site and had to use temperature from the 10 m depth instead of surface temperature for heat flux calculations. The important point, is that our data set covers a fairly wide range of wind stress conditions, up to about 1 Pa (Fig. 2). It is the advantage of our approach that we are able to resolve broad scales of variability, as the response of the mixed layer to surface inputs is nonlinear. The magnitude of wind stress varied greatly over intervals of a few days. Most of the observed variability in the heat loss components are related to variations of the wind stress. Estimated heat loss varied from about -100 to -300 Wm^{-2}.

A contour plot of the observed vertical distribution of water temperature measured at the mooring site is shown in Figure 3. At the beginning of the observations, the water temperature was almost uniform with a value of about 8.2°C. Later, we observe sloping of the isotherms caused by the absorption of solar radiation and transport of heat downward by vertical mixing along with advection of differing water masses. At the end of the experiment in June, water temperature at 10 m exceeded 9.5°C. The temperature structure (see also Fig. 1) suggests that mesoscale processes were significant at times. These processes are primarily manifested in low frequency changes of deep water temperature. However, it should be noted that Gill (1975)

examined mid-ocean eddy activity for several historical weather ship records and found that there was less mesoscale energy at Ocean Station I, near our study site, than at other North Atlantic locations. Our one-dimensional modeling cannot directly account for advection, thus we have attempted to separate the seasonal signal from the mesoscale variability in the experimental data. This was accomplished by subtracting the fluctuations in the deep water temperature (recorded at 150 m depth) from shallower temperature data. This procedure is similar to that of Price *et al.* (1986). The temperature contour obtained in this way (Fig. 4) provides a descriptor of the seasonal changes of the water stability (note that salinity changes were minor).

General features of variability of phytoplankton concentration in the mixed layer throughout the spring season are illustrated in Figures 5a and b. Episodic events of shallowing mixed layer are reflected in some increase of the chlorophyll fluorescence signal. The rate of phytoplankton growth increased significantly during the final weeks of the experiment. Comparison of the bio-optical data with the temperature distribution shown in Figures 1 and 3 indicates that the increase in phytoplankton concentration actually preceded the formation of the seasonal thermocline. This suggests that phytoplankton growth was very sensitive to stability conditions in the water column, and even small increases of the stability may have been sufficient to stimulate the increase of phytoplankton abundance. Interestingly, there were few indications in the past that the spring bloom can be initiated by very low water column stability (e.g., Pingree *et al.,* 1976; Bishop *et al.,* 1986), or even precede the onset of spring temperature stratification (e.g., Colebrook, 1979, 1982; Townsend *et al.,* 1992).

Heat fluxes, pigment concentrations (based on stimulated fluorescence measurements) and the initial *in situ* temperature profile were used as the input data to run the model. The model simulation started with the conditions which occurred on day 103 when the mixed layer was more than 100 m deep. The initial temperature profile was nearly homogeneous over the mixed layer. The simulation domain was 0–740 m, however our focus is on the thermal structure in the upper water layer, where the phytoplankton influence on the spring heating is expected to be important. The modeled temperature distribution is shown in Figure 6a. Importantly, general features of the model results are similar to experimental data (Fig. 4), specifically the onset of acceleration in heating of the mixed layer on about day 145 is well represented by the model.

To illustrate the influence of the phytoplankton bloom on the ML structure, the model was run with the same initial and boundary conditions as before, but assuming low Chl*a* concentration (using the values measured for the day 103, constant in time and equal to 0.2 mg Chl*a* m^{-3} at 10 m depth). The results of the vertical distribution of water temperature from this model simulation are shown in Figure 6b. Generally,

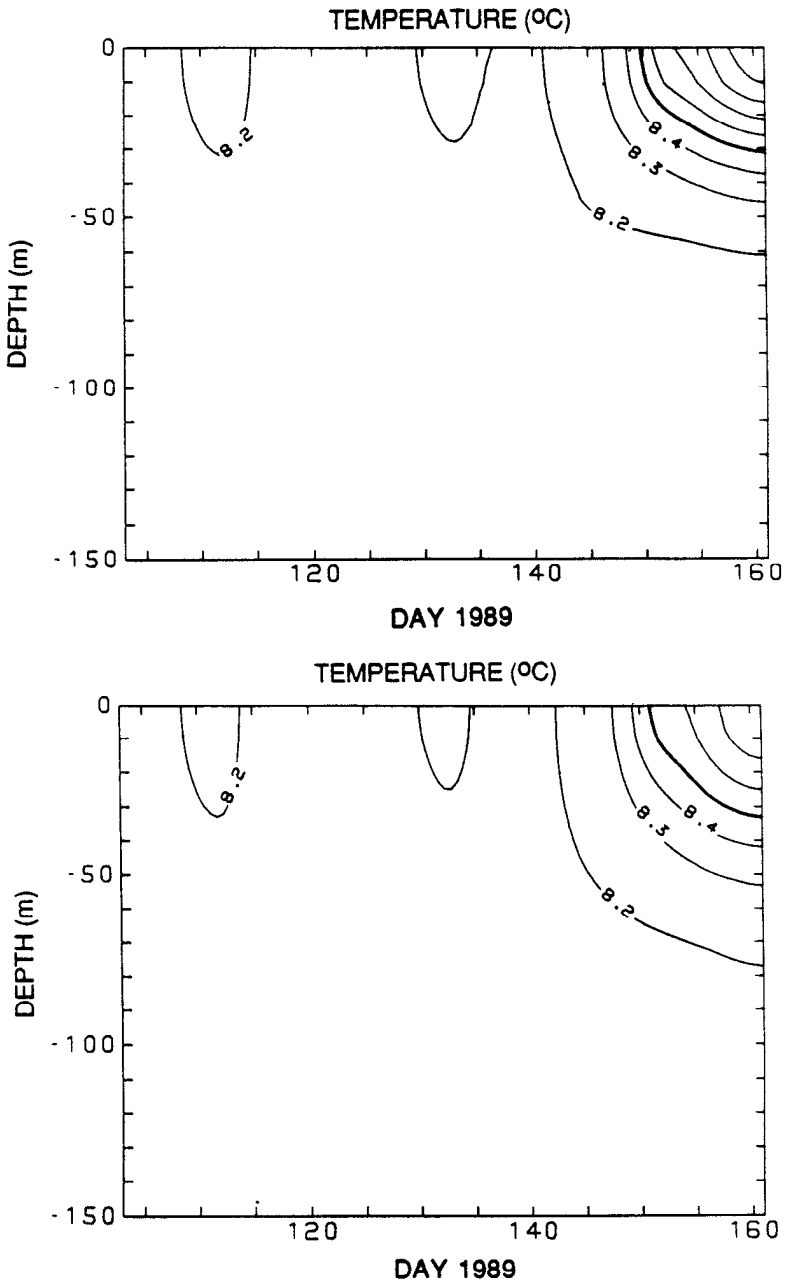

Figure 6. (a) Calculated temperature distribution for model simulation using time series of Chl*a* measured during MLML experiment. (b) Calculated temperature distribution for the model simulation using constant Chl*a* profile (from day 103, ~0.2 mg Chl*a* m^{-3} at 10 m).

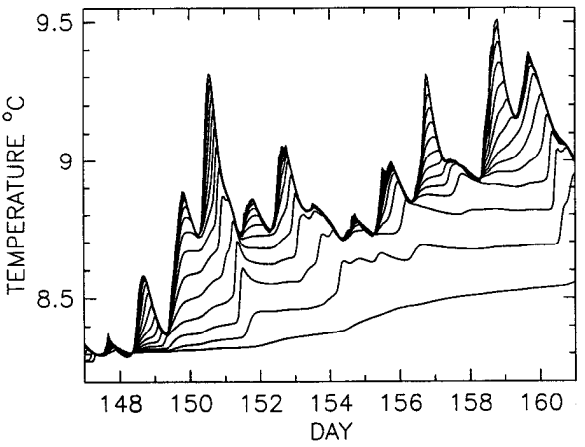

Figure 7. Simulated time series of water temperature (for 0.2, 0.7, 1.3, 2.9, 4.0, 5.2, 6.8, 8.8, 11.1, 14.0, 17.5, 21.8, 27.0, 33.3 m). (a) Calculations done using time series of measured Chl*a* concentration. (b) Calculations done using constant Chl*a* concentration from day 103 (~ 0.2 mg Chl*a* m^{-3}). (c) Superimposed results for days 158–159. Solid line—calculations done using measured Chl*a* time series, dotted line—calculations done using constant Chl*a* profile (from day 103).

under the conditions of higher phytoplankton concentration, the heating rate of the mixed layer is faster than when the concentration was kept low and constant.

The simulated temperature time series (after day 147) at 14 depths in the upper 33 m are shown for two model runs in Figure 7a (using measured Chl*a* concentrations) and Figure 7b (using a constant Chl*a* concentration from day 103). The increase of the phytoplankton concentration from about 0.2 mg Chl*a* m^{-3} to about 2 mg Chl*a* m^{-3} caused, after several days, an increase in the surface water temperature of about 0.2°C. The results from Figures 7a and b for days 158–161 are superimposed in Figure 7c. Note, that the differences involve more efficient heating of the water very close to the surface and slower heating at depth in the case of higher phytoplankton concentration, as opposed to the lower concentration. This results in differing thermal stratifications. The mixed layer depths for the two model runs are compared in Figure 8a. The mixed layer is shallower for the run using measured Chl*a* concentrations (higher values). The difference in the MLD is generally greater at night and as a result the amplitude of the daily variability of MLD is smaller when phytoplankton are more abundant. The differences in the stability structure of the upper water column are also reflected in vertical profiles of the Richardson number (as defined in Eq. 3) shown in Figure 8b for Julian day 151.

Wind speed as well as phytoplankton abundance has an important effect on the thermal structure of the mixed layer. To illustrate this point, the model was run with four constant wind speeds (2, 5, 10, 15 m/s), using heat fluxes as estimated for the MLML experiment, and Chl*a* profiles (constant in time) as measured on days 103

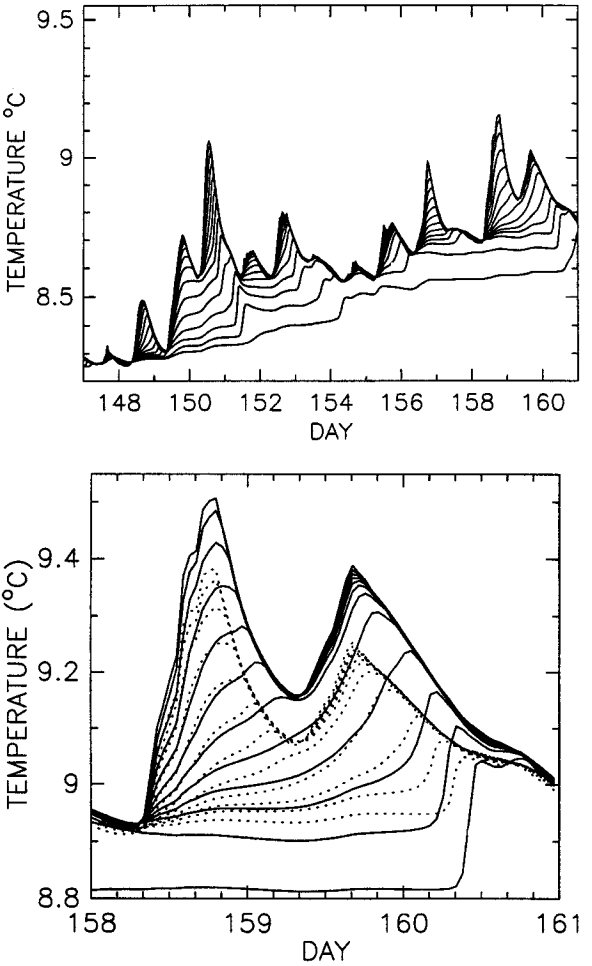

Figure 7. (Continued)

(~0.2 mg Chl*a* m^{-3} at 10 m depth), 150 (~2 mg Chl*a* m^{-3}), twice as high (~4 mg Chl*a* m^{-3}), and 10 times as high as measured on day 150 (~20 mg Chl*a* m^{-3}). The results of the model calculations are shown as time series of temperature (at depths of 0.7, 2, 5, 10, 30, 50, and 110 m) in Figures 9a, b, c, and d. For low wind speed (2 m/s) the surface temperature can be as much as 2°C higher for waters with high phytoplankton concentration than for waters with low phytoplankton concentration. Increasing wind speed causes increasing mixing of the surface water and tends to counteract the effect of increased nonuniformity of heating in the water column. Thus the influence of the phytoplankton concentration on the ML temperature is more significant when low or moderate wind speeds prevail. However, the development of phytoplankton blooms is expected to coincide with such wind conditions, and

the phytoplankton are likely to be important for the ML thermal stratification during these periods.

5. Discussion and conclusions

Our study was stimulated by the observation that the onset of the spring bloom apparently occurred before the formation of the seasonal thermocline. The observation that the spring bloom may precede the seasonal stratification of the surface water, surprising in the light of the classical bloom models, is supported by other experimental data (Colebrook, 1979, 1982; Townsend *et al.,* 1992). It seems that the development of the bloom is very sensitive to even small changes of the water column stability (see also Pingree *et al.,* 1976; Bishop *et al.,* 1986; 1992), but the classical Sverdrup model does not include all the details necessary to understand the temporal evolution of the bloom in its initial phase. As a first step to better understanding the relationship between mixed layer structure and phytoplankton biomass, we have evaluated the role of the bloom on the heating rate of the water column.

The influence of the optical properties of the water on the heating rate has been considered before in the literature. Simpson and Dickey (1981a, b), and Dickey and Simpson (1983) investigated the significance of the downward irradiance parameterization for the upper ocean dynamical structure. These authors applied Mellor-Yamada turbulence scheme and discussed several irradiance parameterizations. They concluded that the vertical distribution of radiative flux in the water column is important for the mixed layer structure for winds <10 m/s. Zaneveld *et al.* (1981) and Lewis *et al.* (1983, 1990) studied the importance of phytoplankton concentration for the heating rate within the mixed layer using simple heat budget equations. However, they did not fully consider dynamical processes which are expected to modify spatial nonuniformities in heating rate. Simonot *et al.* (1988) modeled the role of a phytoplanktonic bloom on sea surface temperature. The biological influence on the sea surface temperature has also been discussed for the climatology of Arabian Sea (Sathyendranath *et al.,* 1991). Since these latter two studies employed bulk dynamical models, they could only include the radiation flux within the ML in the integrated form.

For our study we chose to adapt the Mellor-Yamada turbulence model because of its capacity to include vertical distribution of irradiance. In addition, the stability dependent eddy viscosity and diffusivity parameters allow an interaction between water heating and dynamics. An important modification of the model is the detailed parameterization of the light penetration into the water. The dynamical model was coupled to the pigment-dependent model of spectral attenuation coefficient for downwelling irradiance (Morel, 1988). To our knowledge, this is the first attempt to quantify the effect of a developing bloom on the increase of the water stability by considering vertical distribution of heat gains and losses and spectral attenuation of light by phytoplankton.

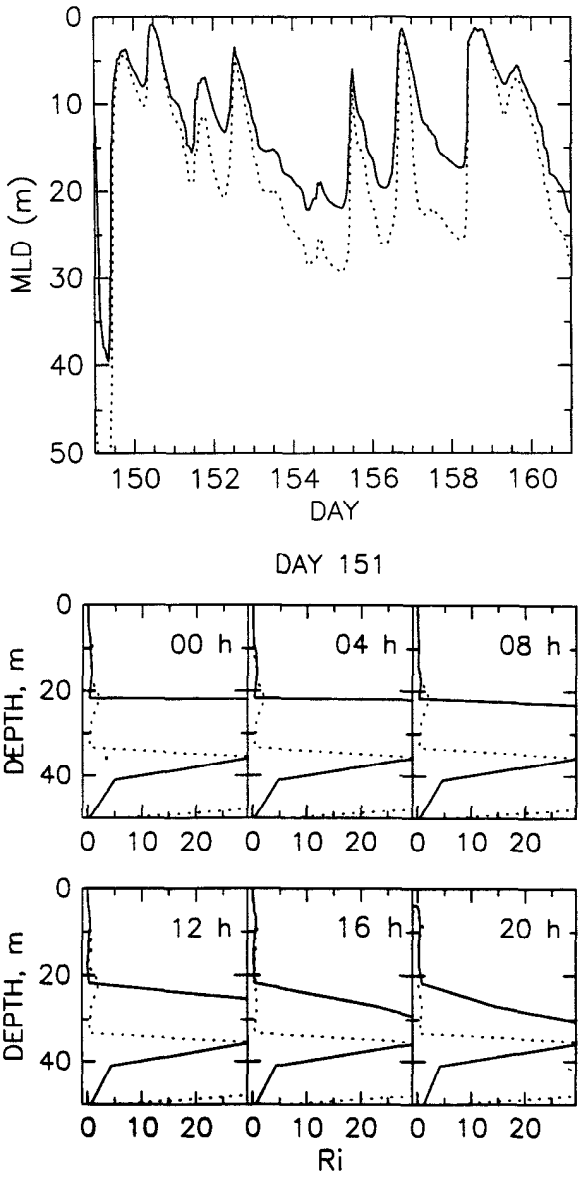

Figure 8. (a) Modeled mixed layer depth (b) Richardson number profiles for day 151. Solid line represents the results for calculations using time series of measured Chl*a* concentration; dotted line—constant constant Chl*a* profile (from day 103).

For the calculations, we chose the situation where surface temperature was not expected to be affected by the phytoplankton in an extremely dramatic way as the phytoplankton concentrations were moderate (about 2–3 mg/m^3 during most of the bloom period covered by our study) and wind speeds were variable. However, we

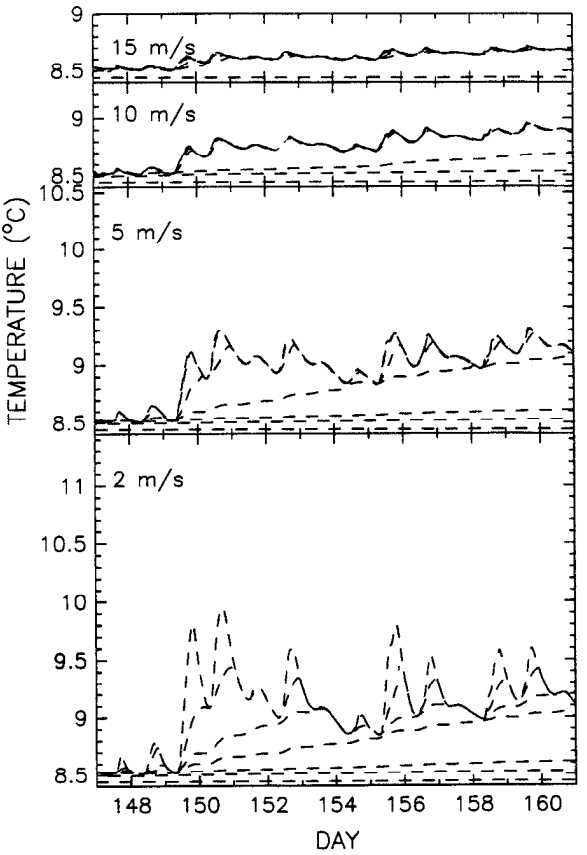

Figure 9. Simulated time series of the temperature (at 0.7, 2, 5, 10, 30, 50, 110 m depths). The model runs were done using constant wind speeds (2, 5, 10, 15 m/s) and heat fluxes estimated during MLML experiment. (a) Using Chl*a* profile from day 103 (~0.2 mg Chl*a* m^{-3} at 10 m), (b) using Chl*a* profile from day 150 (about 2 mg Chl*a* m^{-3} at 10 m depth) (c) using Chl*a* concentration twice as high as measured on day 150 (about 4 mg Chl*a* m^{-3} at 10 m depth), and (d) using Chl*a* concentration 10 times as high as measured on day 150 (about 20 mg Chl*a* m^{-3} at 10 m depth).

have estimated that under these conditions, the increase of phytoplankton abundance during the spring induced an increase of the sea surface temperature by about 0.2°C at the site of our mooring. While MLML results are probably typical for the high latitude open ocean conditions with variable winds and moderate phytoplankton concentration, the biological effect on the mixed layer structure is potentially much more important when vertical mixing is weaker (light winds) and phytoplankton concentrations are higher. By comparing model simulations for four hypothetical phytoplankton concentrations, we found a dramatic increase of the heating rate close to the sea surface water, which led to differences in the surface temperature as great

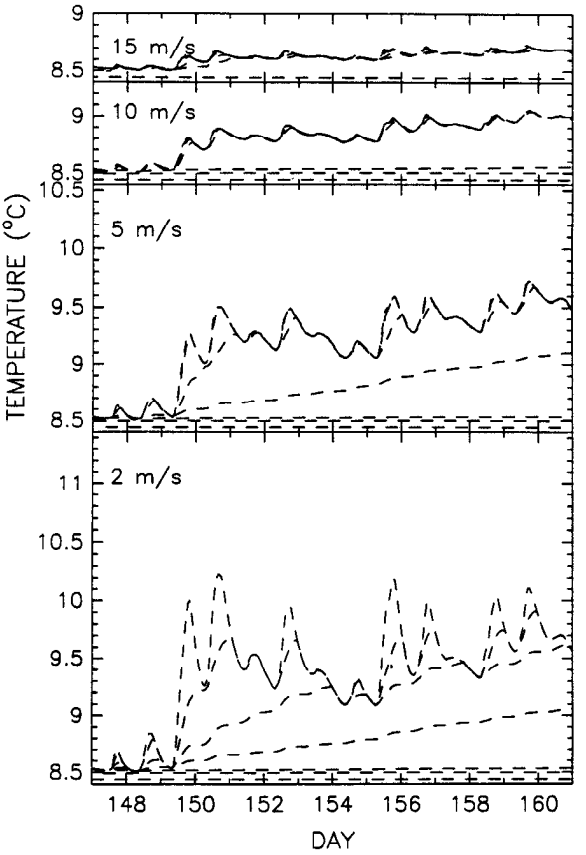

Figure 9. (Continued)

as 2°C between the cases of low and high Chl*a* concentrations (0.2 mg Chl*a* m^{-3} and 20 mg Chl*a* m^{-3}, respectively).

Our model describes vertical mixing and heating processes driven by local surface fluxes of heat and momentum. In actual environmental conditions, local processes are superimposed on the ambient oceanic variability which can be influenced by other processes. These include advection due to mean currents, eddies, planetary and internal waves and Ekman pumping. Mesoscale effects were apparent in our experimental data and not negligible. However, as suggested by Gill (1975), the seasonal temperature signal can be considered separately from mesoscale variability in the vicinity of the mooring site. The increase of the surface water thermal stratification during the spring warming event is relatively well reproduced by the model. There is some uncertainty in our model simulation because of particular assumptions and parameterizations of the surface fluxes. Nevertheless, these difficulties do not alter the main conclusion of our calculations; that is phytoplankton can

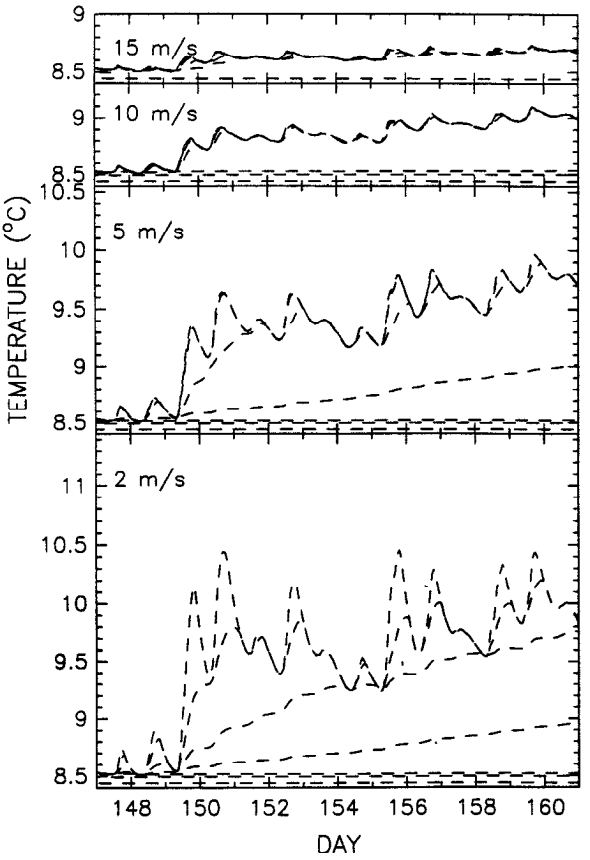

Figure 9. (Continued)

significantly influence the spring evolution of the mixed layer. This conclusion is based on comparison of two model simulations, which use exactly the same boundary conditions but different phytoplankton concentrations. Thus, the differences in the heating rate of the water column in these two cases result only from differences in the attenuation of the visible light related to developing bloom.

The redistribution of the heat flux in the water column with the increase of phytoplankton concentration is associated with stronger thermal stratification and increased water stability. This results in shallower mixed layers and smaller amplitudes of the daily variations of mixed layer depth. It is natural to expect that these changes in the mixing dynamics will in turn influence the rate of phytoplankton growth and losses by removal to greater depths. Such changes will also have some impact on other physical processes, including the air-sea heat exchange and current structure.

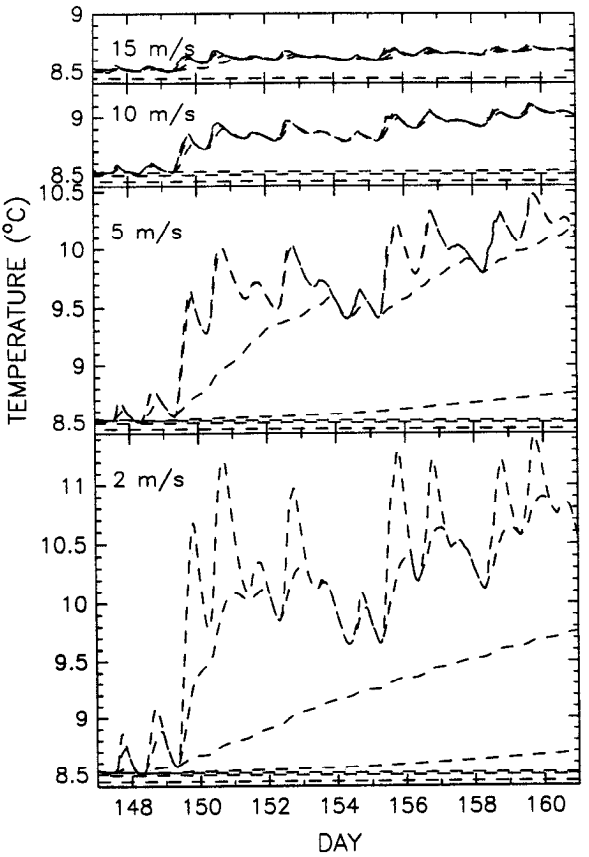

Figure 9. (Continued)

Acknowledgments. This research was sponsored by the Office of Naval Research as part of the Marine Light in the Mixed Layer program (contract no. N00014-89-J-1498). We thank John Marra, Chris Langdon, Bob Weller, and Al Plueddemann for sharing portions of their MLML data, and George Heimerdinger for help in making data from OSV Lima available. Special thanks are due Derek Manov for providing high quality technical assistance during and after the experiment.

REFERENCES

Baker, K. S. and R. C. Smith. 1982. Bio-optical classification and model of natural waters. Limnol. Oceanogr., *27,* 500–509.

Bartz, R., R. Spinrad and J. C. Kitchen. 1988. A low power, high resolution, *in situ* fluorometer for profiling and moored applications in water. Proc. Soc. Photo-Optical Eng., *925,* Ocean Optics IX, 157–170.

Bartz, R., J. R. V. Zaneveld and H. Pak. 1978. A transmissometer for profiling and moored observations in water. Proc. Soc. Photo-Optical Eng., *160,* Ocean Optics V, 102–108.

Bird, R. E. 1984. A simple, solar spectral model for direct-normal and diffuse horizontal irradiance. Solar Energy, *32,* 461–471

Bird, R. E., R. L. Hulstrom and L. J. Lewis. 1983. Terrestrial solar spectral data sets. Solar Energy, *30,* 563–573.

Bishop, J. K. B. 1986. The correction and suspended particulate matter calibration of Sea Tech transmissometer data. Deep-Sea Res., *33,* 121–134.

Bishop, J. K. B., M. H. Conte, P. H. Wiebe, M. R. Roman and C. Langdon. 1986. Particulate matter production and consumption in deep mixed layers: observation in a warm-core ring. Deep-Sea Res., *33,* 1813–1841.

Bishop, J. K. B., R. C. Smith and K. S. Baker. 1992. Springtime distribution and variability of biogenic particulate matter in Gulf Stream warm-core ring 82B and surrounding N.W. Atlantic waters. Deep-Sea Res., *39,* (Suppl. 1A), S295–S325.

Blumberg, A. F. and G. L. Mellor. 1983. Diagnostic and prognostic circulation studies of the South Atlantic Bight. J. Geophys. Res., *88,* 4579–4592.

Booth, C. R. 1976. The design and evaluation of a measurement system for photosynthetically active quantum scalar irradiance. Limnol. Oceanogr., *19,* 326–335.

Bunker, A. F. 1976. Computations of surface energy flux and annual air-sea interaction cycles of the North Atlantic Ocean. Mon. Weather Rev., *104,* 1122–1140.

Colebrook, J. M. 1979. Continuous plankton records: seasonal cycles of phytoplankton and copepods in the North Atlantic Ocean and North Sea. Mar. Biol., *51,* 23–32.

—— 1982. Continuous plankton records: seasonal variations in the distribution of plankton in the North Atlantic and the North Sea. J. Plankton Res., *4,* 435–462.

Dickey, T. D., T. Granata, J. Marra, C. Langdon, J. Wiggert, Z. Chai-Jochner, M. Hamilton, J. Vazquez, M. Stramska, R. Bidigare and D. Siegel. 1993. Seasonal variability of bio-optical and physical properties in the Sargasso Sea. J. Geophys. Res., *98,* 865–898.

Dickey, T. D., J. Marra, T. Granata, C. Langdon, M. Hamilton, J. Wiggert, D. Siegel and A. Bratkovich. 1991. Concurrent high resolution bio-optical and physical time series observation in the Sargasso Sea during the spring of 1987. J. Geophys. Res., *96,* 8643–8664.

Dickey, T. D. and J. J. Simpson. 1983. The influence of optical water type on the diurnal response of the upper ocean. Tellus, *35B,* 142–154.

Emery, W. J. and J. S. Dewar. 1982. Mean temperature-salinity, salinity-depth and temperature-depth curves for the North Atlantic and the North Pacific. Prog. Oceanogr., *11,* 219–305.

Fung, I. Y., D. E. Harrison and A. A. Lacis. 1984. On the variability of the net longwave radiation at the ocean surface, Rev. Geophys. Space Phys., *22,* 177–193.

Geernaert, G. L. 1990. Bulk parameterization for the wind stress and heat fluxes, *in* Surface Waves and Fluxes, *1,* Current Theory, Geernaert, G. L. and W. J. Plant, eds., Kluwer Academic Publishers, 332 pp.

Gill, A. E. 1975. Evidence for mid-ocean eddies in weather ship records. Deep-Sea Res., *22,* 647–652.

Gran, H. H. and T. Braarud. 1935. A quantitative study of the phytoplankton in the Bay of Fundy and the Gulf of Maine. J. Biol. Bd. Canada, *1,* 279–467.

Jerlov, N. G. 1976. Marine Optics. Elsevier, New York, 229 pp.

Kirk, J. T. O. 1983. Light and Photosynthesis in Aquatic Ecosystems. Cambridge University Press, New York, 396 pp.

Kishino, M., N. Okami, M. Takahashi and S. E. Ichimura. 1986. Light utilization efficiency and quantum yield of phytoplankton in a thermally stratified sea. Limnol. Oceanogr., *31,* 557–566.

Langdon, C. 1984. Dissolved oxygen monitoring system using a pulsed electrode: design, performance and evaluation. Deep-Sea Res., *31,* 1357–1367.

Large, W. G. and S. Pond. 1982. Sensible and latent heat flux measurements over the ocean. J. Phys. Oceanogr., *12,* 464–482.

Lewis, M. R., M. E. Carr, G. C. Felman, W. Esaias and Chuck McClain. 1990. Influence of penetrating solar radiation on the heat budget of the equatorial Pacific Ocean. Nature, *347,* 543–545.

Lewis, M. R., J. J. Cullen and T. Platt. 1983. Phytoplankton and thermal structure in the upper ocean: consequences of the nonuniformity in chlorophyll profile. J. Geophys. Res., *88,* 2565–2570.

Marra, J., T. Dickey, W. S. Chamberlin, C. Ho, T. Granata, D. A. Kiefer, C. Langdon, R. Smith, K. Baker, R. Bidigare and M. Hamilton. 1992. The estimation of seasonal primary production from moored optical sensors in the Sargasso Sea. J. Geophys. Res., *97,* 7399–7412.

Mazumder, A., W. D. Taylor, D. J. McQueen and D. R. S. Lean. 1990. Effects of fish and plankton on lake temperature and mixing depth. Science, *247,* 312–315.

Mellor, G. L. and P. A. Durbin. 1975. The structure and dynamics of the ocean surface layer. J. Phys. Oceanogr., *5,* 718–728.

Mellor, G. L. and T. Yamada. 1974. A hierarchy of turbulence closure models for planetary boundary layers. J. Atmos. Sci., *31,* 1791–1806.

—— 1982. Development of a turbulence closure model for geophysical fluid problems. Rev. Geophys. Space Phys, *20,* 851–875.

Morel, A. 1988. Optical modeling of the upper ocean in relation to its biogenous matter content (Case 1 waters). J. Geophys. Res., *93,* 10,749–10,768.

Palmer, K. F. and D. Williams. 1974. Optical properties of water in the near infrared. J. Opt. Soc. Amer., *64,* 1107–1110.

Payne, R. E. 1972. Albedo of the sea surface. J. Atmos. Sci., *29,* 959–970.

Pingree, R. D., P. M. Holligan, G. T. Mardell and R. N. Head. 1976. The influence of physical stability on spring, summer and autumn phytoplankton blooms in the Celtic Sea. J. Mar. Biol. Assoc. U.K., *56,* 845–873.

Price, J. F., R. A. Weller and R. Pinkel. 1986. Diurnal cycling: Observations and models of the upper ocean response to diurnal heating, cooling, and wind mixing. J. Geophys. Res., *91,* 8411–8427.

Richtmyer, R. D. and K. W. Morton. 1967. Difference Methods for Initial-Value Problems. Interscience, 405 pp.

Roll, H. U. 1965. Physics of the Marine Atmosphere. Academic Press, New York, 426 pp.

Sathyendranath, S., A. D. Gouvela, S. R. Shetya, P. Ravindran and T. Platt. 1991. Biological control of surface temperature in the Arabian Sea. Nature, *349,* 54–56.

Sathyendranath, S. and T. Platt. 1988. The spectral irradiance field at the surface and in the interior of the ocean: A model for applications in oceanography and remote sensing. J. Geophys. Res., *93,* 9270–9280.

Siegel, D. A. and T. D. Dickey. 1987. On the parameterization of irradiance for the open ocean photoprocesses. J. Geophys. Res., *92,* 14,648–14,662.

Simonot, J.-Y., E. Dollinger and H. Le Treut. 1988. Thermodynamics-biological-optical coupling in the oceanic mixed layer. J. Geophys. Res., *93,* 8193–8202.

Simpson, J. J. and T. D. Dickey. 1981a. The relationship between downward irradiance and upper ocean structure. J. Phys. Oceanogr., *11,* 876–882.

—— 1981b. Alternative parameterizations of downward irradiance and their dynamical significance. J. Phys. Oceanogr., *11,* 876–882.

Smith, R. C. and K. S. Baker. 1981. Optical properties of the clearest natural waters. Appl. Opt., *20,* 177–184.

—— 1986. Analysis of ocean optical data, II. Proc. Soc. Photo-Optical Eng., *637,* 95–107.

Stramska, M. and T. D. Dickey. 1992. Variability of bio-optical properties of the upper ocean associated with diel cycles in phytoplankton population. J. Geophys. Res., *97,* 17,873–17,887.

Sverdrup, H. U. 1953. On conditions of the vernal blooming of phytoplankton. J. Cons. Int. Explor. Mer, *18,* 287–295.

Townsend, D. W., M. D. Keller, M. E. Sieracki and S. G. Ackleson. 1992. Spring phytoplankton blooms in the absence of vertical water column stratification. Nature, *360,* 59–62.

Weller, R. A. and R. E. Davis. 1980. A vector measuring current meter. Deep-Sea Res., *27,* 565–582.

Woods, J. D. and W. Barkmann. 1986. The response of the upper ocean to solar heating. I. The mixed layer. Quart. J. Royal Meteorol. Soc., *112,* 1–27.

Zaneveld, J. R., J. C. Kitchen and H. Pak. 1981. The influence of optical water type on the heating rate of a constant depth mixed layer. J. Geophys. Res., *86,* 6426–6428.

Received: *8 September, 1992;* revised: *11 May, 1993.*